Available online at www.sciencedirect.com

ScienceDirect

Procedia Engineering 12 (2011) 1–8

Engineering Procedia

2011 SREE Conference on Engineering Modeling and Simulation (CEMS 2011)

Finite element analysis method for horizontal well hydraulic fracturing

Zhang Guangming[a,b]*, Xiong Chunming[a,b], Liu Jiandong[a,b], Lin Ju[a, b], Shen Luhe[a,b]

[a] Research Institute of Petroleum Exploration & Development, PetroChina, Beijing 100083, China
[b] Key Laboratory of Oil & Gas Production, CNPC, Beijing 100083, China

Abstract

Horizontal well hydraulic fracturing is a complex technology and there is unclear understanding about the mechanics of hydraulic fracturing. The Fluid-solid coupling elements were employed to describe the behavior of rock, and the pore pressure cohesive elements were employed to simulate the process of fracture initiation and propagation. The fluid flow in the fractures and fracturing fluid leak-off effects were also taken into account. By adopting field data, the staged fracturing process of a horizontal well in Daqing Oilfield, China was simulated. The simulated results are fit well with the field treatment data.

Keywords: Horizontal well; hydraulic fracturing; Finite element; Fracture; Fluid-solid coupling

1. Introduction

Hydraulic fracturing can be broadly defined as the process by which a fracture initiates and propagates due to hydraulic loading applied by a fluid inside the fracture. Even in the most basic form, hydraulic fracturing is a complicated process to model, as it involves the coupling of at least three processes [1]: (1) the mechanical deformation induced by the fluid pressure on the fracture surfaces; (2) the flow of fluid pressure on the fracture surfaces; (3) the fracture initiation and propagation.

Due to the complication of hydraulic fracturing, mathematical solutions are impossible. Usually, numerical simulation methods are used to study the behaviors of hydraulic fracturing, however, many

* Corresponding author. Tel.: +86-010-83593250
E-mail address: gmzhang@petrochina.com.cn.

1877–7058 © 2011 Published by Elsevier Ltd. Open access under CC BY-NC-ND license.
doi:10.1016/j.proeng.2011.05.002

assumptions and simplifications are made in many model to solve the problem of complicated hydraulic fracturing. Perkins and Kern [2] adapted the classic Sneddon plane strain crack solution to develop the so-called PK model. Later, Nordgren [3] adapted the PK model to formulate the PKN model, which included the effects of fluid loss. Khristianovic and Zheltov, and Geertsma and de Klerk [4] independently developed the so-called KGD (plane strain) model. Pseudo-3D (P3D) model [5] and planar 3D (PL3D) model [6, 7] are based on PKN model and KGD model, and also have a few of assumptions and simplifications. There have also been attempts to model fully 3D hydraulic fractures [8] with limited success. The computational burden on such coupled systems is still excessive, even with today's powerful computational resources.

Varieties of numerical methods [9-13] have been developed for hydraulic fracture simulations. With the fast development of computer technology over the past decades, the finite element analysis method is more and more used in geotechnical engineering. In this paper, a non-linear full fluid-solid coupling finite element model was proposed with the finite element software ABAQUS, the fluid-solid coupling theory is used to capture the behavior of rock, the damage mechanics criterion is adopted to simulate the fracture initiation and propagation. The fluid flow in the fractures and fracturing fluid leak-off effect are also taken into account. Based on the field data, the finite model was established and the staged fracturing process of a horizontal well in Daqing Oilfield, China was simulated with the model.

2. The basic equations

2.1 Fluid-solid coupling equation of rock

Equilibrium can be written in the form of virtual work principle for the volume under its current configuration at time t as [14]

$$\int_V (\bar{\boldsymbol{\sigma}} - p_w \mathbf{I}) : \delta\boldsymbol{\varepsilon} \mathrm{d}V = \int_S \mathbf{t} \cdot \delta\mathbf{v} \mathrm{d}S + \int_V \mathbf{f} \cdot \delta\mathbf{v} \mathrm{d}V \tag{1}$$

Where $\bar{\boldsymbol{\sigma}}$ and $\delta\boldsymbol{\varepsilon} = \mathrm{sym}(\partial\delta\mathbf{v}/\partial\mathbf{x})$ are effective stress and virtual rate of deformation respectively, p_w is the pore pressure, $\mathbf{t}$ and $\mathbf{f}$ are the surface traction per unit area and body force per unit volume respectively, $\mathbf{I}$ is unit matrix.

2.2 Continuity equation of liquid flow in porous medium

A porous medium is modelled in ABAQUS by attaching the finite element mesh to the solid phase. Liquid can flow through the mesh. Equating the time rate of change of the total mass of wetting liquid in the control volume V to the mass of wetting liquid crossing the surface S per unit time gives the wetting liquid mass continuity equation in the following form

$$\frac{\mathrm{d}}{\mathrm{d}t}\left(\int_V \rho_w n_w \mathrm{d}V\right) + \int_S \rho_w n_w \mathbf{n} \cdot \mathbf{v}_w \mathrm{d}S = 0 \tag{2}$$

Where ρ_w, n_w and $\mathbf{v}_w$ are the mass density of the liquid, the porosity of the medium and the average velocity of the liquid relative to the solid phase (the seepage velocity) respectively, $\mathbf{n}$ is the outward normal to

The liquid flow is described by Darcy's law as

$$\mathbf{v}_w = -\frac{1}{n_w g \rho_w} \boldsymbol{k} \cdot \left(\frac{\partial p_w}{\partial \mathbf{x}} - \rho_w \boldsymbol{g}\right) \tag{3}$$

Where $\boldsymbol{k}$ and $\boldsymbol{g} = -g\partial z / \partial \mathbf{x}$ are the permeability of the medium and the gravitational acceleration respectively.

2.3 Damage model of cohesive element in ABAQUS

Cohesive element is used to simulate the behavior of rock fracture in software ABAQUS. The constitutive response of cohesive element is characterized by a traction-separation law. The initial response of cohesive element is assumed to be linear before damage initiation. However, once the traction in a cohesive element reaches the damage initiation value, material damage occurs according to a damage evolution law. The traction acting on cohesive element monotonically degrades as the separation displacement between the two outer surfaces of cohesive element increases after damage initiation. Fig.1 depicts the evolution of the relationship between traction and separation of cohesive element.

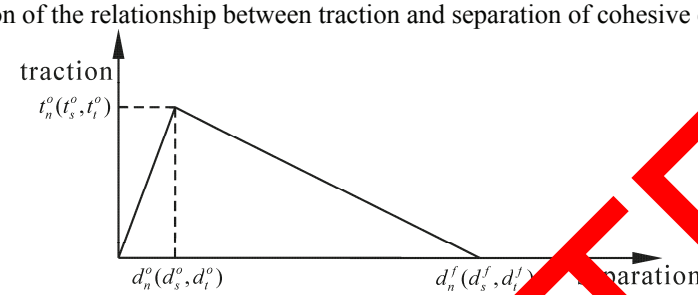

Fig.1 Typical traction-separation response

2.3.1 Damage initiation criterion of cohesive element

Damage initiation refers to the beginning of degradation of the response of a material. Damage is assumed to initiate when a quadratic interaction function involving the ratios of stresses (tractions) reaches the value of one. This criterion can be expressed as [15]

$$\left\{\frac{\langle t_n\rangle}{t_n^o}\right\}^2+\left\{\frac{t_s}{t_s^o}\right\}^2+\left\{\frac{t_t}{t_t^o}\right\}^2=1 \tag{4}$$

Where t_n, t_s and t_t represent the normal and the two shear tractions, respectively. t_n^o, t_s^o, and t_t^o represent the tensile strength and shear strengths in the corresponding directions, respectively. The symbol $\langle\rangle$ signifies that a pure compressive deformation or stress state does not initiate damage.

2.3.2 Damage evolution law of cohesive element

The damage evolution law describes the degradation of material stiffness once the corresponding damage initiation criterion is reached. A scalar damage variable, D, represents the overall damage in the material. It is initially equal to 0. The variable D monotonically increases from 0 to 1 as damage developing. The stress component in the traction-separation model is affected by the damage according to the following expression

$$t_n=\begin{cases}(1-D)\,\bar{t}_n & \bar{t}_n\ge 0\\ \bar{t}_n & \text{otherwise}\end{cases} \tag{5}$$

Where $\bar{t}_n$ is the stress component predicted by the linear elastic behavior without damage and the current strain value.

For linear softening, the scalar damage variable, D is expressed with the following form [16]

$$D=\frac{d_n^f(d_n^{\max}-d_n^o)}{d_n^{\max}(d_n^f-d_n^o)} \tag{6}$$

Where d_n^f and d_n^o are the opening displacements at complete failure and at the initiation of damage, respectively, $d_n^{\max}$ refers to the maximum value of opening displacement attained during the loading history.

2.4 Flow within cohesive element

The fluid flow model in the cohesive element enables the fluid pressure on the cohesive element surface to be incorporated in the modeling of hydraulically driven fractures. The fluid cohesive response comprises the tangential flow within the fracture and the normal flow across the fracture. The flow patterns of pore fluid in cohesive element are depicted in Fig.2.

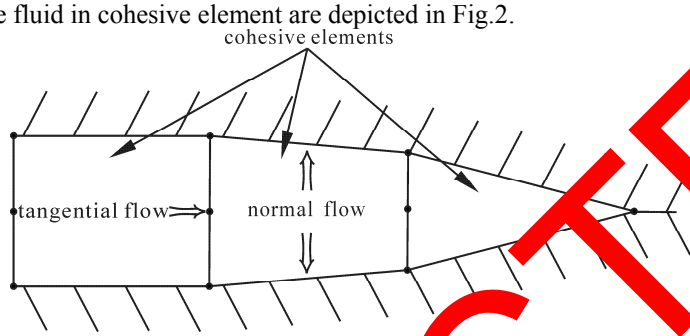

Fig.2 The flow patterns of pore fluid in cohesive elements

2.4.1 Tangential flow

The tangential flow in cohesive element is described with the following equation.

$$\boldsymbol{q}d = -\frac{d^3}{12\mu}\nabla p \tag{7}$$

Where $\boldsymbol{q}$ is the volume flow rate density vector, d is the opening displacement of the two outer surfaces, ∇p is the pressure gradient along the cohesive element, μ is the fluid viscosity.

2.4.2 Normal flow

The normal flow is described as

$$\begin{cases} q_t = c_t(p_i - p_t) \\ q_b = c_b(p_i - p_b) \end{cases} \tag{8}$$

Where q_t and q_b are the flow rates in the top and bottom surfaces of cohesive element, respectively, c_t and c_b are the leak-off coefficients on the top and bottom surfaces, respectively, p_i is the internal pressure of cohesive element, p_t and p_b are the pore pressures on the top and bottom surfaces, respectively.

3. Simulation model

A staged fracturing process of a horizontal well in Daqing Oilfield, China is simulated with the software ABAQUS. The field data of Daqing Oilfield are adopted in computation. The true vertical depth of the well is 1592.05 m, the drilled well depth is 2345 m. Provided that the shape of hydraulic fracture is axial symmetry about the wellbore center line, it will be needed to establish a finite element model only containing half of the meridian ellipse, as depicted in Fig.3. The dimension of the model is 300 m and

200 m in the X, Y directions, respectively. Perforation, wellbore, cement sheath, reservoir, micro-annulus and transverse fracture are included in the model. The diameter of perforation is 8.8 mm, the outer diameter and the thickness of wellbore is 139.7 mm and 7.72 mm, respectively. The outer diameter of cement casing is 200 mm. In-situ stresses of reservoir in the X, Y directions, are -11.8 MPa, -21.8 MPa, respectively. The saturation and the porosity of formation is 1 and 0.2, respectively. The initial pore pressure of formation is 14 MPa. All the normal direction displacements of outer boundary surfaces of the model are restricted and the outer boundary keeps 14 MPa pore pressure during the process of simulation. The elastic modulus and poisson's ratio of wellbore are 210 GPa and 0.3, respectively. The elastic modulus and poisson's ratio of cement sheath are 30 GPa and 0.25, respectively. The reservoir geologic parameters and the material properties of cohesive element in transverse fracture and micro-annulus are listed in Table 1 and Table 2, respectively. Number of nodes and elements in the numerical model are 79 622 and 77 653, respectively.

Table 1
Reservoir geologic parameters

	elastic modulus (GPa)	poisson's ratio	permeability (mD)	fluid specific gravity ($N \cdot m^{-3}$)
Reservoir	35	0.22	2	8624

Table 2
Material properties of cohesive element in transverse fracture and micro-annulus

	elastic modulus (GPa)	t_n^o (MPa)	t_s^o (MPa)	t_t^o (MPa)	d_n^f (mm)
transverse fracture	35	4	1.5	1.5	5
micro-annulus	35	0	2	2	5

Cohesive elements are embedded in reservoir to describe the process of transverse fracture initiation and propagation during treatment history. Cohesive elements are embedded between cement casing and pay zone to catch the behavior of micro-annulus fracture. Transverse fracture will initiate and propagate according to the principle of least principal stress. Transverse fracture and micro-annulus fracture both connect to the perforation, so they could initiate and propagate simultaneously under the injected hydraulic loading. All the cohesive elements are undamaged and the opening displacements are zero initially. The fractures volume increase as cohesive elements damage and fail according to the damage initiation criterion and corresponding damage evolution law and a typical T-shaped fracture is likely to occur.

The treatment design also considers a pumping schedule for both fluid and proppants. As the proppant-laden fluid is injected, there will be an interaction of solid particles and fluid. Consideration of these effects in detail is challenging, it is a common practice to "lump" all these effects into a modified viscosity of the slurry, which is usually expressed as [17]

$$\mu = \mu_0 \times (1 - c / 0.65)^{-1.7} \tag{9}$$

Where μ is the viscosity of proppant-laden fluid, c is proppant concentration.

ABAQUS field variable technology and user subroutine UFIELD are used to implement equation (9).

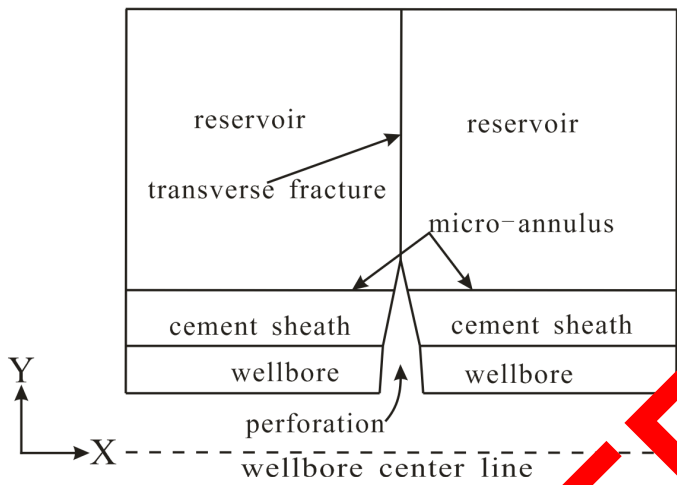

Fig.3 Schematic plot of the model

4. Results and discussion

The radial fracture geometry is obtained because the finite element model is axis symmetry about wellbore center line. Fig.4 presents pore pressure distribution and the fracture configuration at the final moment of treatment history. The deformation magnification factor is taken 400 and the axis symmetry model is revolved 180 around the wellbore center line for crack observation of the simulation results. At the beginning of simulation, cohesive elements between micro-annulus and in transverse direction damage simultaneously, a T-shaped fracture generates. At the later time, micro-annulus disappears due to the large stress concentration factor near wellbore. Then only the transverse fracture remains and propagates. The half length and width of the transverse fracture are 98.1 m and 10.34 mm, respectively.

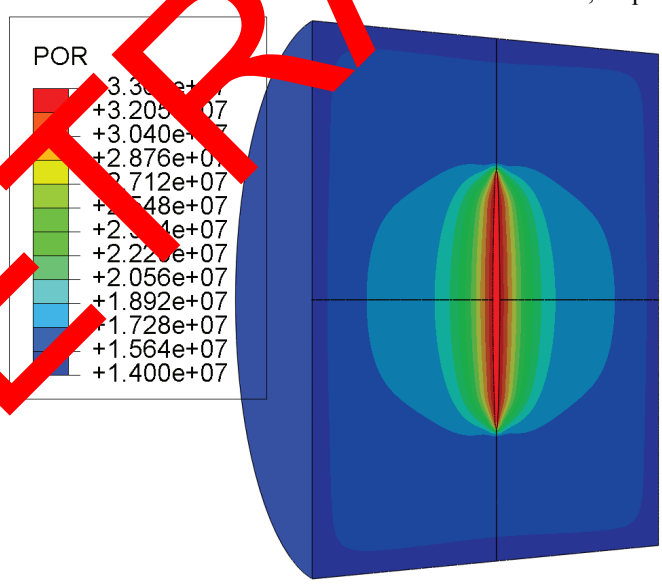

Fig.4 Pore pressure distribution in the model at the final moment of treatment history

Fracturing fluid is pumped into the wellbore, part of fracturing fluid leaks into formation and the other leaves in the fracture. Fracturing fluid leaks into formation, which results in increasing formation pore pressure, formation effective stress increases according to the effective stress principle of porous medium. When the formation effective stress rises up to formation tensile strength, hydraulic fracture initiates and propagates forward a small distance, which produces a new fracture tip, in which the formation effective stress is lower than the formation tensile strength. Hydraulic fracture will not propagate until the effective stress at the new fracture tip reaches the formation tensile strength again. As more fracturing fluid is injected into the fracture, the width of fracture enlarges and the effective stress at the new fracture tip increases. Hydraulic fracture will propagate once more when the effective stress at the new fracture tip reaches the formation tensile strength. When the normal stress of a cohesive element rises up to the tensile strength, the cohesive element initiates damage and with further loading the stiffness of cohesive element decreases monotonically as depicted in Fig.1.

Fracturing fluid flow rate keeps 3.46 m^3/min and lasts for about 30 min. The results of the simulated and field measured treatment history are plotted in Fig.5. The proppant concentration and fracturing fluid flow rate in simulation are taken as the same as in the field implementation process (presented also in Fig.5). The evolution of the bottomhole pressure obtained from the simulation is consistent very well with the corresponding field data, which approves the validation of the proposed finite element model. The evolution of bottomhole pressure is the most important judgment of success or failure of a hydraulic fracturing treatment. The obtained results demonstrate that the proposed model is applicable to hydraulic fracturing designs and treatments for reservoirs lithology similar to Daqing Oilfield, China.

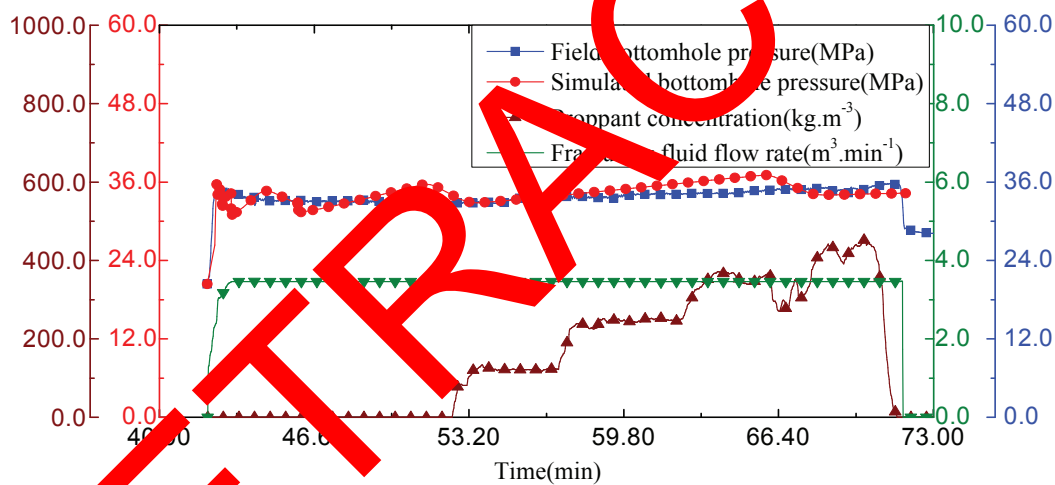

Fig.5 Curves of field treatment history and simulated bottomhole pressure history

5. Conclusions

Hydraulic fracturing analysis is inherently a complicated problem, in which fluid flow, deformation of porous medium and fracture initiation and propagation are fully coupled, mathematical solutions are impossible. Usually, Numerical simulation method is employed to catch and study the characters in the process of hydraulic fracturing. Finite element analysis (FEA) has been approving an effective method to simulate and forecast the process of hydraulic fracturing.

Multiple transverse fractures can be generated in the process of horizontal well hydraulic fracturing, the stimulation effect is more considerable than vertical well. It is significant to study the mechanics of horizontal well hydraulic fracturing.

A non-linear fluid-solid coupling finite element model was established with the finite element software ABAQUS. A staged fracturing process of a horizontal well in Daqing Oilfield, China is simulated with the model. The initiation and propagation of hydraulic fractures are simulated by using the cohesive element based on damage mechanics. A good match between simulation results and field measurement data is obtained. Validation of the numerical model is approved.

References:

[1] Adachi, J., Siebrits, E., Peirce, A., Desroches, J., 2007. Computer simulation of hydraulic fractures. International Journal of Rock Mechanics & Mining Sciences. 44(5): 739-757.

[2] Perkins, T.K., Kern, L.R., 1961. Widths of hydraulic fractures. Journal of Petroleum Technology. 13(9): 937-949.

[3] Nordren, R.P., 1972. Propagation of a vertical hydraulic fracture. SPE J. 12(8): 306-314.

[4] Geertsma, J., de Klerk, F., 1969. A rapid method of predicting width and extent of hydraulically induced fractures. Journal Petroleum Technology. 21: 1571-1581.

[5] Weng, X.W., 1992. Incorporation of 2D fluid into a pseudo-3D hydraulic fracturing simulator. SPE Production Engineering. 7(4): 331-337.

[6] Siebrits, E., Peirce, A.P.,2002. An efficient multi-layer planar 3D fracture growth algorithm using a fixed mesh approach. Internal Journal for Numerical Methods in Engineering. 53:691-717.

[7] Jeffrey, R.G., Bunger, A.P., 2007. A detailed comparison of experimental and numerical data on hydraulic fracture height growth though stress contrasts. SPE Paper 106030, 2007 SPE Hydraulic Fracturing Technology Conference, College Station, Texas, U.S.A. Jan.29-31.

[8] Setaari, A., Cleary, M.P.,1984. Three-dimensional simulation of hydraulic fracturing. Journal of Petroleum Technology. 36(7): 1177-1190.

[9] Fischer, M.P., Gross, M.R., Engelder, T., Greenfield, R.J., 1994. Finite-element analysis of the stress distribution around a pressurized crack in a layered elastic medium: implications for the spacing of fluid-driven joints in bedded sedimentary rock. Tectonophysics. 247(1): 49-64.

[10] Siebrits, E., Gu, H.R., Desroches, J., 2001. An improved pseudo-3D hydraulic fracturing simulator for multiple layered materials. Proceeding of 10th International Conference on Computer Methods and Advances in Geomechanics. Tucson, USA. Jan.7-12.

[11] Smith, M.B., Bale, A.B., Britt, J.K., Klein, H.H., Dang, X., 2001. Layered modulus effects on fracture propagation, proppant placement and fracture modeling. SPE Paper 71654, 2001 SPE Annual Technical Conference and Exhibition, New Orleans, Louisiana, USA. Sep.30-Oct.3.

[12] Miskimins, J.L., Barree, R.D., 2003. Modeling of hydraulic fracture height containment in laminated sand and shale sequences. SPE Paper 80935, 2003 SPE Production and Operations Symposium, Oklahoma, USA. Mar.22-25.

[13] Hustedt, B., Bruwarts, D., Bjoerndal, K.P., Masfry, R., van den Hoek, P.J., 2006. Induced fracturing in reservoir simulation: application of a new coupled simulator to a waterflooding field example. SPE Paper 102467, 2006 SPE Annual Technical Conference and Exhibition, San Antonio, Texas, USA. Sep.24-27.

[14] Xue, B., Wu, A., Wang, X., Lian, Z.L., Zhang, J., Zhang, S.C., 2006. A Three-Dimensional Finite Element Model of Hydraulic Progressive Damage, Key Engineering Material. 324-325, 375-378.

[15] Camanho, P.P., Davila, C.G., 2002. Mixed-mode decohesion finite elements for the simulation of delamination in composite materials. NASA/TM-2002-211737, 1-42.

[16] Turon, A., Camanho, P.P., Costa, J., Davila, C.G., 2006. A damage model for the simulation of delamination in advanced composites under variable-model loading. Mechanics of Materials. 38(11): 1072-1089.

[17] Barree, R.D., Conway, M.W., 1994. Experimental and numerical modeling of convective proppant transport. SPE Paper 28564, 1994 SPE Annual Technical Conference and Exhibition, New Orleans, USA. Sep.25-28.